

Target Tracking using Robust Sensor Motion Control

Jingwei Hu^a, Dave Zachariah^a, Petre Stoica^a

^a*Department of Information Technology, Uppsala University, Uppsala, Sweden*

Abstract

We consider the problem of tracking moving targets using mobile wireless sensors (of possibly different types). This is a joint estimation and control problem in which a tracking system must take into account both target and sensor dynamics. We make minimal assumptions about the target dynamics, namely only that their accelerations are bounded. We develop a control law that determines the sensor motion control signals so as to maximize target resolvability as the target dynamics evolve. The method is given a tractable formulation that is amenable to an efficient search method and is evaluated in a series of experiments involving both round-trip time based ranging and Doppler frequency shift measurements.

1. Introduction

Tracking the positions of moving objects (aka. targets) using wireless signals is a classical estimation problem [1, 7], in which the ability to track crucially depends on the spatial configuration of targets and sensors. The targets can be unmanned aerial vehicles, aircraft or land vehicles. The development of wireless technologies has enabled the flexible deployment of sensors and, consequently, the potential of finding favourable sensor configurations in a given application.

In the case of *static targets*, one important line of work is that of optimal sensor placement, which uses the Fisher Information Matrix (FIM) and associated metrics to quantify the ability to resolve a target [6, 11, 24, 25]. Sensors that are mobile, or in other ways dynamically reconfigurable, can be used to improve target localization sequentially. This is illustrated in [13], which

Email addresses: `jingwei.hu@it.uu.se` (Jingwei Hu), `dave.zachariah@it.uu.se` (Dave Zachariah), `ps@it.uu.se` (Petre Stoica)

considers the problem of designing a control law for a single bearings-only sensor. The proposed control law is based on maximizing the determinant of the (estimated) FIM using a first-order method. An alternative case with multiple ranging sensors is considered in [9], where a distributed algorithm is developed for steering the sensors along the boundary of a convex set containing the target.

In the case of *dynamic targets*, the optimal sensor configurations change dynamically. In [21], a fuzzy-logic based method is developed for distributed sensor control using point estimates of a single target. The estimates are obtained using distributed Kalman filters under the assumption of a linear measurement model. Tracking using mobile sensors requires an appropriately designed control law, since their motion towards a currently favourable configuration may become unfavourable at the time they reach it. This includes taking into account estimation errors, as exemplified in [10] which considers the problem of tracking using aerial vehicles equipped with position measuring sensors. In the cited paper, sensor control is based on reducing the estimated error covariance matrix obtained from a Kalman filter using a first-order method. A robust approach that takes into account the least favourable target trajectories as well as measurement noise realizations is developed in [26]. The sensor control uses a receding horizon formulation to minimize the trace of the Kalman filter error covariance matrix at the end of the time horizon. The control law is implemented by gridding the target action and noise realization spaces, and then performing a minimax tree search. While increasing robustness, the computational complexity of the minimax tree grows prohibitively with the time horizon, even when utilizing gridding and pruning techniques.

In this work, we develop a tracking framework to determine a robust control law for mobile sensors that

- is applicable to various (and possibly mixed) sensor types,
- aims at continually improving target resolvability,
- takes into account target uncertainty over a receding time horizon while employing minimal assumptions about the targets, and
- can be implemented efficiently using first-order methods.

We formulate the sensor control law that aims to minimize an expected Cramér-Rao bound (CRB) using a computationally efficient first-order method.

Figure 1a demonstrates the proposed framework for tracking two targets using three ranging sensors that are confined to a rectangular perimeter. The tracking system uses a maximum likelihood estimator and only assumes an upper bound a_{\max} on the accelerations of the targets, which move in an unknown coordinated manner. The sensors are initialized at the center of the perimeter resulting in poor localization capabilities. Figure 1b shows the position errors over time. We can see that after overcoming the challenging sensor initialization, the system drives the errors down towards their corresponding ‘noise floors’ as indicated by the corresponding CRB.

Next, we turn to setting up the formal problem that this paper addresses. We then turn to developing a joint estimation and control method. Finally, a statistical evaluation of the proposed method is provided for a few different scenarios with aerial vehicles using mixed sensor types.

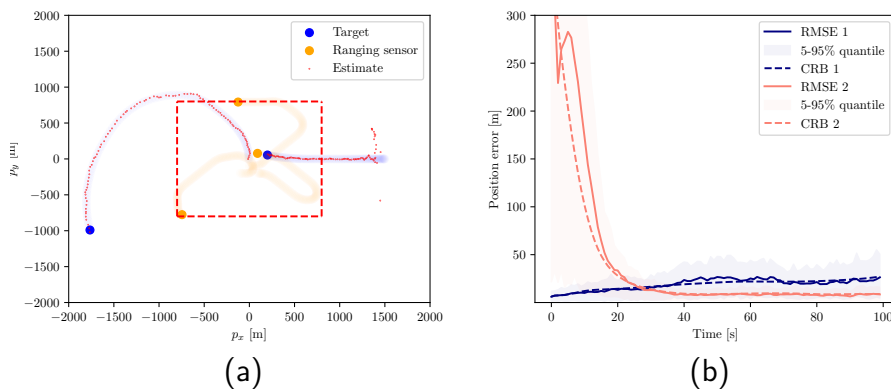


Figure 1: Proposed tracking system using sensor motion control. $N = 2$ targets are tracked in two-dimensional space ($d = 2$) using $M = 3$ sensors that measure the ranges to the targets. Target and sensor accelerations are assumed to be bounded by $a_{\max} = 5 \text{ m/s}^2$ and $u_{\max} = 2 \text{ m/s}^2$, respectively. The sensor errors are specified in Section 4.1. (a) The targets move in an unknown, coordinated manner. The sensors are initially positioned at the center of the perimeter (dashed in red) and can move freely within this boundary. One target moves from the center of the perimeter toward the outside, while the other moves inward, entering the perimeter. (b) The resulting tracking position errors over time. For reference, we have included the Cramér-Rao (CRB) bounds, which show that the errors are driven down to their respective ‘noise floors’ determined by the sensor configuration. Details about the experiments are specified in Section 4.

2. PROBLEM FORMULATION

We consider the problem of tracking N targets using M mobile sensors. Consider a target n observed by a sensor m . Their positions and velocities in d -dimensional space ($d = 2$ or 3) are *states* denoted

$$\mathbf{x}^n = \begin{bmatrix} \mathbf{p}^n \\ \mathbf{v}^n \end{bmatrix} \quad \text{and} \quad \mathbf{s}^m = \begin{bmatrix} \tilde{\mathbf{p}}^m \\ \tilde{\mathbf{v}}^m \end{bmatrix}, \quad (1)$$

respectively.

At time t , sensor m provides a measurement of target n , which we denote $y_t^{m,n}$. The sensors may be of different types, providing, for instance, round-trip time or frequency shift measurements, which we will consider below.

In the case of ranging measurements, the mean round-trip time from sensor m to target n , and back, is

$$\mathbb{E}[y_t^{m,n}] = \frac{2}{c} \|\mathbf{I}_d \mathbf{0}\| (\mathbf{x}_t^n - \mathbf{s}_t^m)_2, \quad (2)$$

where c is the speed of light. In the case of Doppler frequency shift measurements, the mean observation is

$$\mathbb{E}[y_t^{m,n}] = -\frac{f_c \sum_{i=1}^d (x_i^n - s_i^m)(x_{d+i}^n - s_{d+i}^m)}{c \|\mathbf{I}_d \mathbf{0}\| (\mathbf{x}^n - \mathbf{s}^m)_2}, \quad (3)$$

where f_c is the carrier frequency [22] and the index i denotes the i th element of the target and sensor.

Both target n and sensor m can be in motion, which we describe using a general discrete-time model. For target n , we have:

$$\mathbf{x}_t^n = \underbrace{\begin{bmatrix} \mathbf{I} & dt\mathbf{I} \\ \mathbf{0} & \mathbf{I} \end{bmatrix}}_{\mathbf{F}} \mathbf{x}_{t-1}^n + \underbrace{\begin{bmatrix} \frac{1}{2}dt^2\mathbf{I} \\ dt\mathbf{I} \end{bmatrix}}_{\mathbf{G}} \mathbf{a}_t^n, \quad (4)$$

where dt denotes the sampling period, \mathbf{a}^n is the acceleration vector of the target. For sensor m , we have:

$$\mathbf{s}_t^m = \underbrace{\begin{bmatrix} \mathbf{I} & dt\mathbf{I} \\ \mathbf{0} & \mathbf{I} \end{bmatrix}}_{\tilde{\mathbf{F}}} \mathbf{s}_{t-1}^m + \underbrace{\begin{bmatrix} \frac{1}{2}dt^2\mathbf{I} \\ dt\mathbf{I} \end{bmatrix}}_{\tilde{\mathbf{G}}} \mathbf{u}_t^m, \quad (5)$$

where \mathbf{u}^m is the acceleration vector of the mobile sensor. The trajectory of the target is unknown. For the sake of robustness, we will make *minimal* assumptions and consider only physical constraints on its unknown acceleration:

$$\|\mathbf{a}_t^n\|_2 \leq a_{\max}. \quad (6)$$

The mobile sensor acceleration is a *control input* that we can design subject to certain constraints: Firstly, it is bounded

$$\|\mathbf{u}_t^m\|_2 \leq u_{\max}. \quad (7)$$

and, secondly, the sensor must often stay within a certain perimeter or respect certain velocity limits described by the set of box constraints

$$\{\mathbf{s}_t^m : \mathbf{s}_{\min} \leq \mathbf{s}_t^m \leq \mathbf{s}_{\max}, \forall t\}. \quad (8)$$

The problem we face is to coordinate the motion of M sensors so as to track target all N accurately. More specifically, given measurements obtained from all sensors at time t , our aim is to design the subsequent control input \mathbf{u}_{t+1}^m so that a target state estimator $\hat{\mathbf{x}}_{t+1}^n$ will perform well for all n .

Remark 1: It is possible to split the problem into N independent single-target problems by assigning groups of sensors to each target. However, this would require, e.g., $M \geq 3N$ ranging sensors, which precludes the scenario illustrated in Figure 1a. In contrast, the cooperative multi-target approach requires only $M \geq 3$ and avoids the problem of assigning groups of sensors to different targets.

Remark 2: We assume here that the correspondence between measurement and target is resolved. Data association is, however, an important challenge. Probabilistic methods such as the Joint Probabilistic Data Association (JPDA)[5] resolve ambiguous measurements by marginalizing over feasible associations without maintaining explicit hypotheses. To enhance scalability, loopy belief propagation (LBP)[23] offers approximate inference over graphical models. In parallel, hypothesis-based methods like Multiple Hypothesis Tracking (MHT)[2, 15], which maintains and prunes trees of association hypotheses, and its sampling variant MCMCDA [12], explore the association space through explicit hypothesis management or stochastic sampling. More recently, learning-based methods [3, 18] have emerged as data-driven generalizations: while inspired by the structural principles classic approaches, they depart from their underlying probabilistic formulations by approximating association through neural inference. While these methods are relevant,

the focus of this paper is on cooperative sensor control for informative data acquisition under constraints.

3. Method

For notational convenience, we introduce the sensor state *configuration*:

$$\mathbf{s}_t = \begin{bmatrix} \mathbf{s}_t^1 \\ \vdots \\ \mathbf{s}_t^M \end{bmatrix} \quad (9)$$

Our tracking method is based on the maximum likelihood estimator (MLE). Let \mathbf{y}_t^n denote the vector of all measurements of target n at time t and assume it follows a Gaussian data model $\mathbf{y}_t^n \sim \mathcal{N}(\boldsymbol{\mu}(\mathbf{x}^n, \mathbf{s}_t), \boldsymbol{\Sigma}(\mathbf{x}^n, \mathbf{s}_t))$, where the mean and covariance depend both on the known sensor configuration and the unknown target state. Suppose we have an unbiased prediction $\check{\mathbf{x}}_t^n$ with an error covariance matrix $\check{\mathbf{C}}_{n,t}$. Using \mathbf{y}_t^n and $\check{\mathbf{x}}_t^n$ as two sources of data, we have the maximum likelihood estimator of the target state:

$$\begin{aligned} \hat{\mathbf{x}}_t^n = \arg \min_{\mathbf{x}^n} & \|\mathbf{y}_t^n - \boldsymbol{\mu}(\mathbf{x}^n, \mathbf{s}_t)\|_{\boldsymbol{\Sigma}^{-1}(\mathbf{x}^n, \mathbf{s}_t)}^2 + \ln |\boldsymbol{\Sigma}(\mathbf{x}^n, \mathbf{s}_t)| \\ & + \|\mathbf{x}^n - \check{\mathbf{x}}_t^n\|_{\check{\mathbf{C}}_{n,t}^{-1}}^2, \quad n = 1, \dots, N, \end{aligned} \quad (10)$$

where we have used the least favorable distribution for the prediction $\check{\mathbf{x}}_t^n \sim \mathcal{N}(\mathbf{x}_t^n, \check{\mathbf{C}}_{n,t})$ [16, 14]. The error covariance matrix of the MLE $\hat{\mathbf{x}}_t^n$ is approximated by

$$\mathbf{C}_{n,t} = (\mathbf{J}(\mathbf{x}_t^n, \mathbf{s}_t) + \check{\mathbf{C}}_{n,t}^{-1})^{-1}, \quad (11)$$

when applying a plug-in estimate of the target state [19, 8, 17]. Here \mathbf{J} is the Fisher information matrix given by

$$\begin{aligned} [\mathbf{J}(\mathbf{x}^n, \mathbf{s})]_{ij} &= \frac{\partial \boldsymbol{\mu}(\mathbf{x}^n, \mathbf{s})^\top}{\partial x_i^n} \boldsymbol{\Sigma}^{-1}(\mathbf{x}^n, \mathbf{s}) \frac{\partial \boldsymbol{\mu}(\mathbf{x}^n, \mathbf{s})}{\partial x_j^n} \\ &+ \frac{1}{2} \text{tr} \left\{ \boldsymbol{\Sigma}^{-1}(\mathbf{x}^n, \mathbf{s}) \frac{\partial \boldsymbol{\Sigma}(\mathbf{x}^n, \mathbf{s})}{\partial x_i^n} \boldsymbol{\Sigma}^{-1}(\mathbf{x}^n, \mathbf{s}) \frac{\partial \boldsymbol{\Sigma}(\mathbf{x}^n, \mathbf{s})}{\partial x_j^n} \right\}, \end{aligned}$$

for $i, j = 1, \dots, 2d$ (and dropping the time index for notational brevity).

We consider $\check{\mathbf{x}}_t^n$ to be a k -step prediction. This can be formed using the dynamic model (4): Suppose the unknown \mathbf{a}_t^n in (4) is modeled as a zero-mean random variable with a covariance matrix $\mathbf{Q}(a_{\max})$. Using a uniform

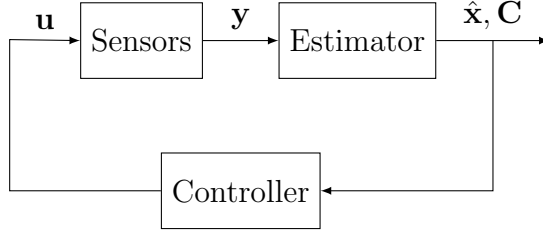


Figure 2: Tracking method with sensor motion control. The sensors provide a snapshot of measurements \mathbf{y} . This is fed to an estimator which provides a point estimate $\hat{\mathbf{x}}$ of the target states and an error covariance matrix, \mathbf{C} . Based on these two quantities, the controller determines the sensor inputs \mathbf{u} for the next time step.

distribution for \mathbf{a}_t^n over $[-a_{\max}, a_{\max}]^d$ yields conservative relaxation of the bound (6) and a covariance matrix

$$\mathbf{Q}(a_{\max}) = \frac{a_{\max}^2}{3} \mathbf{I}_d.$$

Then starting at a prior estimate at time $t - k$, we have the following k -step predictor, $\check{\mathbf{x}}_t^n = \mathbf{F}^k \hat{\mathbf{x}}_{t-k}^n$ with a resulting error covariance matrix (using (5), see [7])

$$\check{\mathbf{C}}_{n,t} = \mathbf{F}^k \mathbf{C}_{n,t-k} (\mathbf{F}^k)^\top + \sum_{i=1}^k \mathbf{F}^{i-1} \mathbf{G} \mathbf{Q} \mathbf{G}^\top (\mathbf{F}^{i-1})^\top, \quad (12)$$

where $\mathbf{C}_{n,t-k}$ is prior error covariance approximated by (11).

An overview of the tracking framework proposed below is illustrated in Figure 2.

3.1. Sensor state configuration and control objective

To plan the sensor trajectories at time t , we are interested in quantifying how the resulting sensor state configuration \mathbf{s}_{t+k} at time $t + k$ will affect the estimation error, defined as

$$\mathbb{E} \left[\|\mathbf{x}_{t+k}^n - \hat{\mathbf{x}}_{t+k}^n\|_{\mathbf{W}}^2 \right] \quad (13)$$

where $\mathbf{W} \succeq \mathbf{0}$ is a weight matrix of choice, e.g.,

$$\mathbf{W} \propto \begin{bmatrix} \mathbf{I}_d & \mathbf{0} \\ \mathbf{0} & dt \mathbf{I}_d \end{bmatrix}, \quad (14)$$

which converts the velocity errors at any time step into equivalent position errors.

Using measurements \mathbf{y}_{t+k}^n and the k -step prediction $\check{\mathbf{x}}_{t+k}^n$ as data, the Cramér-Rao inequality [8, 17, 19] yields an (asymptotically) achievable lower bound on the estimation error (13). Specifically, we consider the expected CRB, by treating \mathbf{x}_{t+k}^n as a random variable:

$$\mathbb{E} \left[\|\mathbf{x}_{t+k}^n - \hat{\mathbf{x}}_{t+k}^n\|_{\mathbf{W}}^2 \right] \geq \mathbb{E} \left[g(\mathbf{x}_{t+k}^n, \mathbf{s}_{t+k}) \right], \quad (15)$$

where

$$g(\mathbf{x}_{t+k}^n, \mathbf{s}_{t+k}) \equiv \text{tr} \left\{ \mathbf{W} (\mathbf{J}(\mathbf{x}_{t+k}^n, \mathbf{s}_{t+k}) + \check{\mathbf{C}}_{n,t+k}^{-1})^{-1} \right\}, \quad (16)$$

the prediction error covariance $\check{\mathbf{C}}_{n,t+k}$ is given by (12) and Thus $\mathbb{E}[g(\mathbf{x}_{t+k}^n, \mathbf{s}_{t+k})]$ in (15) provides a k -step ahead error bound, as a function of the unknown target state and the sensor state configuration. It is this quantity we seek to reduce by controlling the sensor motion. While the CRB becomes tight in the high signal-to-noise ratio regimes, it remains a practical metric for the resolvability of the target states.

We now consider the *feasible* k -step sensor trajectories in order to minimize the expected CRB (15). A joint sequence of control inputs

$$\mathbf{U}_t = \begin{bmatrix} \mathbf{u}_{t+1}^1 & \cdots & \mathbf{u}_{t+k}^1 \\ \vdots & \ddots & \vdots \\ \mathbf{u}_{t+1}^M & \cdots & \mathbf{u}_{t+k}^M \end{bmatrix}$$

determines the sensor state configuration \mathbf{s}_{t+k} (9) via the dynamic model (5). That is, for each sensor m , we have

$$\mathbf{s}_{t+k}^m \equiv \tilde{\mathbf{F}}^k \mathbf{s}_t^m + \sum_{i=1}^k \tilde{\mathbf{F}}^{i-1} \tilde{\mathbf{G}} \mathbf{u}_{t+i}^m. \quad (17)$$

Similarly, the target trajectory starting at \mathbf{x}_t^n is given by

$$\mathbf{x}_{t+k}^n \equiv \mathbf{F}^k \mathbf{x}_t^n + \sum_{i=1}^k \mathbf{F}^{i-1} \mathbf{G} \mathbf{a}_{t+i}^n, \quad (18)$$

where the acceleration must satisfy (6). Note that the target trajectory is treated here as a random variable.

The arguments of $g(\mathbf{x}_{t+k}^n, \mathbf{s}_{t+k})$ in (15) can now be substituted by the target and sensor trajectory variables in (17) and (18):

$$g(\mathbf{x}_t^n, \mathbf{a}_{t+1}^n, \dots, \mathbf{a}_{t+k}^n, \mathbf{U}_t) \equiv g(\mathbf{x}_{t+k}^n, \mathbf{s}_{t+k}), \quad (19)$$

where the target acceleration vectors must satisfy (6) while the control inputs must belong to the set of bounded accelerations

$$\mathcal{U} = \left\{ \mathbf{U}_t : \|\mathbf{u}_{t+k}^m\|_2 \leq u_{\max}, \forall k, m \right\} \quad (20)$$

as well as

$$\mathcal{U}_c = \left\{ \mathbf{U}_t : \mathbf{s}_{\min} \leq \tilde{\mathbf{F}}^k \mathbf{s}_t^m + \sum_{i=1}^k \tilde{\mathbf{F}}^{i-1} \tilde{\mathbf{G}} \mathbf{u}_{t+i}^m \leq \mathbf{s}_{\max}, \forall k, m \right\} \quad (21)$$

for the box constraints (7).

We take the expected CRB (15), together with (19), as our control objective. Specifically, we use the lower bound on the sum of estimation errors for the N targets:

$$\mathbf{U}_t^* = \arg \min_{\mathbf{U}_t \in \mathcal{U} \cap \mathcal{U}_c} \mathcal{J}(\mathbf{U}_t), \quad (22)$$

where

$$\mathcal{J}(\mathbf{U}_t) = \sum_{n=1}^N \mathbb{E}[g(\mathbf{x}_{t+k}^n, \mathbf{a}_{t+1}^n, \dots, \mathbf{a}_{t+k}^n, \mathbf{U}_t)] \quad (23)$$

The control inputs \mathbf{u}_{t+1}^m for each mobile sensor at time t would then be obtained by solving (22). Because the criterion takes into account possible target trajectories, the resulting control method is robust against target uncertainties. Unfortunately, as it stands, (22) is an intractable problem.

Remark: We have chosen the expected CRB in (15) as our metric rather than the *posterior* CRB [19] for computational reasons: Evaluation of the latter for time $t+k$ requires a recursively computed covariance matrix starting from time t , unlike the bound in (15). This makes a posterior-based bound more challenging to optimize with respect to \mathbf{U}_t .

3.2. Approximation and relaxation of optimization problem

To render (22) tractable, we first turn to approximating the criterion (23) and then turn to relaxing the constraints in (20).

To approximate the expectation in the criterion, we use a deterministic sigma-point sampling method to sample possible trajectories $(\mathbf{x}_t^n, \mathbf{a}_{t+1}^n, \dots, \mathbf{a}_{t+k}^n)$. Then the expectation in (23) is replaced by a sample approximation. For notational simplicity, we concatenate the sequence $(\mathbf{x}_t^n, \mathbf{a}_{t+1}^n, \dots, \mathbf{a}_{t+k}^n)$ into a single vector \mathbf{z}_{t+k}^n of dimension $d_z = (2+k)d$. This unknown vector determines the trajectory of target n from time t to $t+k$. Using the sigma-point sampling method, we multiple sample trajectories for target n where the ℓ th sample is given by

$$\mathbf{z}_{t+k,(\ell)}^n = \begin{cases} \bar{\mathbf{z}}_{t+k}^n, & \text{for } \ell = 0 \\ \bar{\mathbf{z}}_{t+k}^n + \eta^{1/2}[\mathbf{P}_{t+k}^{1/2}]_{\ell}, & \text{for } \ell = 1, \dots, d_z \\ \bar{\mathbf{z}}_{t+k}^n - \eta^{1/2}[\mathbf{P}_{t+k}^{1/2}]_{\ell-d_z}, & \text{for } \ell = d_z + 1, \dots, 2d_z + 1 \end{cases} \quad (24)$$

and

$$\bar{\mathbf{z}}_{t+k}^n = \begin{bmatrix} \hat{\mathbf{x}}_t^n \\ \mathbf{0} \end{bmatrix} \quad \mathbf{P}_{t+k}^n = \begin{bmatrix} \mathbf{C}_t^n & \dots & \mathbf{0} \\ \vdots & \ddots & \vdots \\ \mathbf{0} & \dots & \mathbf{Q} \end{bmatrix}. \quad (25)$$

The scaling factor η is set according to the principles in [4]. Then the expectation over possible target trajectories in (23) is approximated by averaging over the $2d_z + 1$ sample trajectories for each target:

$$\mathcal{J}(\mathbf{U}_t) \simeq \sum_{n=1}^N \sum_{\ell=0}^{2d_z+1} g(\mathbf{z}_{t+k,(\ell)}^n, \mathbf{U}_t). \quad (26)$$

To further speed up the solution of (22), we relax the quadratic constraints \mathcal{U} by replacing them with box constraints. Utilizing the fact that $\|\mathbf{u}\|_2 \leq \sqrt{\dim(\mathbf{u})}\|\mathbf{u}\|_\infty$ for any vector \mathbf{z} , we can relax the constraint in (7) into

$$\|\mathbf{u}_t^m\|_\infty \leq \frac{u_{\max}}{\sqrt{d}}.$$

We denote the corresponding set of constraints as \mathcal{U}_∞ .

In sum, we replace the criterion in (22) by the sum (26) and the quadratic constraint \mathcal{U} by \mathcal{U}_∞ so that:

$$\mathbf{U}_t^* = \arg \min_{\mathbf{U}_t \in \mathcal{U}_\infty \cap \mathcal{U}_c} \sum_{n=1}^N \sum_{\ell=0}^{2d_z+1} g(\mathbf{z}_{t+k,(\ell)}^n, \mathbf{U}_t), \quad (27)$$

Since $d_z = (2 + k)d$, the computational demand scales linearly with k but the problem is rendered tractable due to the independence of terms and the possibility of efficient gradient computations.

Since all constraints become linear, we apply a computationally efficient interior-point solver to solve (27). Since linear independence constraint qualification holds, the Karush-Kuhn-Tucker conditions are also necessary for a local optimum. Then interior-point methods will converge under standard regularity conditions that the cost function (30) is differentiable and that its Hessian is positive definite near at the local optimum [20]. Problem (27) is nonconvex and we cannot assert any global optimality properties. This is, however, less of a concern as long as any local optimum continually maneuver the sensors toward better configurations.

The resulting tracking system, summarized in Figure 2, is described in Algorithm 1 below.

Algorithm 1 Tracking with sensor motion control

joint_estimate_control(\mathbf{y}_t) :

$(\hat{\mathbf{x}}_t, \mathbf{C}_t) \leftarrow \text{estimator}(\mathbf{y}_t)$

$\{\mathbf{u}_{t+1}^m\} \leftarrow \text{robust_control}(\hat{\mathbf{x}}_t, \mathbf{C}_t)$

return $\hat{\mathbf{x}}_t, \mathbf{C}_t, \{\mathbf{u}_{t+1}^m\}$

robust_control($\hat{\mathbf{x}}_t, \mathbf{C}_t$) :

 Sample trajectories from $\hat{\mathbf{x}}_t, \mathbf{C}_t$ using (24)

 Obtain solution \mathbf{U}_{t+1}^* to (27) using interior-point solver.

return $\{\mathbf{u}_{t+1}^{m,*}\}$

4. NUMERICAL EXPERIMENTS

We present a series of numerical experiments that demonstrate the ability of the proposed method to maintain good tracking performance, using different sensor types and even when starting with unfavourable configurations. We benchmark the statistical performance of the proposed tracking method using a CRB based on a zero-mean random acceleration model. This is a useful but slightly conservative bound.

On a standard laptop, the computation of the control input at each time t takes approximately 2 seconds, thus demonstrating the tractability of the

method. The code implementation is available here ¹.

The controller has one main user parameter, the prediction horizon k . The choice of k depends on the sampling period of the controller relative to the target dynamics, and its maximum value is limited by computational constraints. For all examples, we set $k = 6$, unless stated otherwise.

4.1. Measurement models

We consider two types of wireless sensors in the experiments. First, we use ranging based on round-trip time measurements, as in (2), with distance-dependent measurement noise variance for sensor m :

$$\sigma^2(\mathbf{x}^n, \mathbf{s}^m) = \frac{\sigma_{\text{range}}^2}{c^2} (1 + \lambda \mu^2(\mathbf{x}^n, \mathbf{s}^m)) \quad (28)$$

where $c = 3 \cdot 10^8$ [m/s], $\sigma_{\text{range}} = 1$ [m] and $\lambda = 0.01$ are constants. Secondly, we use sensors that measure Doppler frequency shifts [22] as described in (3) with a carrier frequency f_c of 2.3 GHz. Here we consider a noise model for sensor m :

$$\sigma^2(\mathbf{x}^n, \mathbf{s}^m) \equiv \sigma_{\text{Doppler}}^2 \quad (29)$$

with a standard deviation of 1 [Hz]. The sensors are assumed to be calibrated such that the constants are known.

4.2. Three ranging sensors tracking in 2D space

We begin with a simple scenario in two-dimensional space ($d = 2$) using only ranging measurements, for which we have some prior intuition. We know that a target position is identifiable provided $M = 3$ sensors are well separated and that the achievable accuracy improves by maintaining a large angle of separation between them. At the same time, an increased distance to the target affects the signal-to-noise ratio adversely. Therefore the tracking system must find an appropriate balance between these factors.

To better illustrate the controller’s performance, we initialize the sensors at the same location for two different scenarios. In the first scenario, depicted in Figure 3a, the target moves from the center of the perimeter to the bottom left outside. The sensors quickly respond by adjusting their positions. Once sufficiently separated, one sensor moves in the direction of the target, while

¹<https://github.com/jingwei91hu/ActiveTracking>

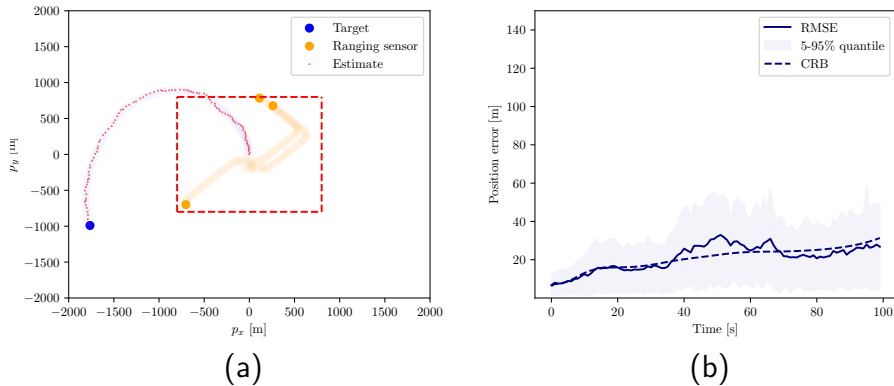


Figure 3: (a) Ranging sensors tracking a single target in 2D space. (b) The resulting tracking position errors over time. $u_{\max} = 2 \text{ m/s}^2$ and $a_{\max} = 5 \text{ m/s}^2$. The results are to be compared with the multitarget case in Figure 1.

the other two move orthogonally to the first sensor so as to improve the target resolvability. This dynamic sensor configuration consistently maintains relatively low tracking errors. Since the target is leaving the perimeter, the overall tracking error inevitably increases, but the sensor motions slow down this degradation.

The second scenario, shown in Figure 1a, is more challenging, as an additional target enters the perimeter from the outside. Initially, the sensors are poorly positioned relative to the new target, resulting in a highly biased estimate. The controller adapts the sensor geometry by splitting roles: one sensor moves to cover the newly entered target while the others maintain coverage of the left-hand target, avoiding the suboptimal configuration that would arise if all sensors moved in the same direction. This adaptation in geometry plays a key role in reducing the estimation error for both targets as the configuration improves. Comparing the multitarget and single target cases in Figures 1b and 3b, we observe a similar tracking performance of the same target.

We now study the robustness formulation used in (27). What is the gain of averaging over multiple possible target trajectories as compared to a simpler method that uses a single-point prediction of each trajectory? That

is,

$$\mathbf{U}_t^{**} = \arg \min_{\mathbf{U}_t \in \mathcal{U}_\infty \cap \mathcal{U}_c} \sum_{n=1}^N g(\hat{\mathbf{x}}_t^n, \mathbf{0}, \dots, \mathbf{0}, \mathbf{U}_t) \quad (30)$$

where $\hat{\mathbf{a}}_i^n \equiv \mathbf{0}$ is the optimal point prediction of the future acceleration vectors. We consider the challenging scenario depicted in Figure 4a and compare the tracking errors of the robust and certainty-equivalent systems over 100 Monte Carlo runs. As shown in Figure 4b, the expected CRB obtained from the single-point based design is notably worse during a period. Moreover, the tracking performance is severely degraded after approximately $t \geq 50$ when the sensor trajectories have failed to adequately resolve the target at some point and the MLE is stuck in a poor minimum as a result. This illustrates the robustness of sigma-point based approach as compared to a method that fails to take into account the uncertainty of the target trajectory.

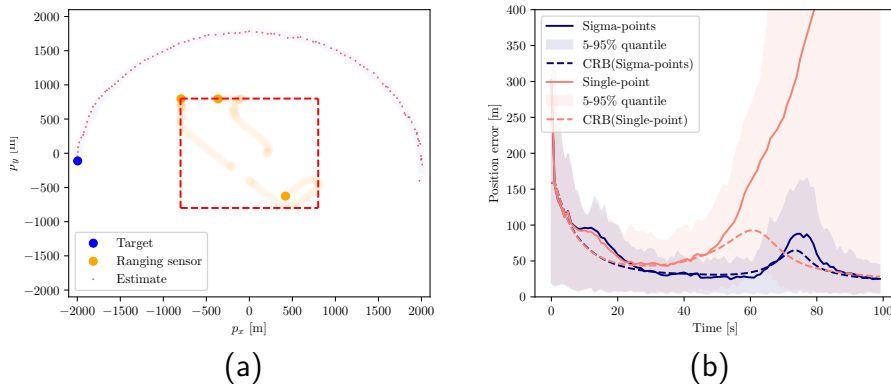


Figure 4: Comparison between using sigma-point and single-point based approximations of the criterion (23), cf. (27) and (30). (a) Scenario illustration tracking a single target. (b) Performance measures of sigma-point versus single-point approximations, using 100 Monte Carlo simulations. The solid curve denotes RMSE. $u_{\max} = 2 \text{ m/s}^2$ and $a_{\max} = 5 \text{ m/s}^2$.

Finally, we study the effect of specifying the acceleration bound u_{\max} as well as the prediction horizon k . Figure 5a compares a realistic acceleration bound of $a_{\max} = 5 \text{ m/s}^2$ with an overly conservative bound of $a_{\max} = 500 \text{ m/s}^2$. As expected, the conservative choice reduces the influence of prior estimates in the state update, leading to a slightly higher error variance. Nevertheless, continual sensor reconfiguration keeps the tracking error low. Figure 5b compares prediction horizons $k = 2, 4, 6$. A longer

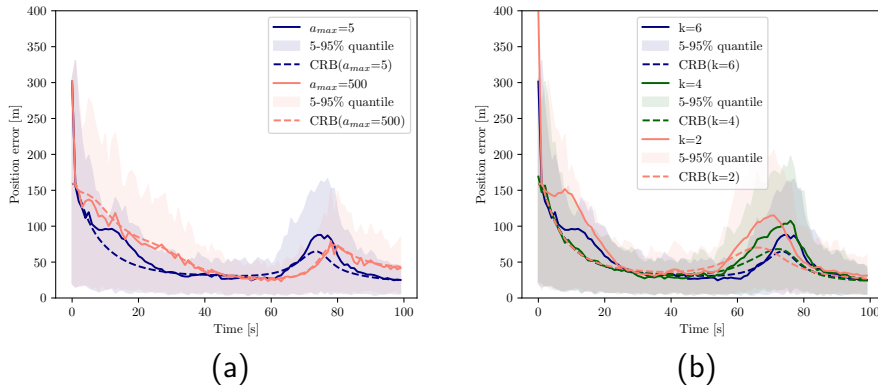


Figure 5: (a) Comparison between using acceleration bound $a_{\max} = 5\text{m/s}^2$ versus the conservative $a_{\max} = 500\text{m/s}^2$. (b) Comparison between prediction horizons $k = 2, 4$ and 6 . Both cases use configuration in the scenario of Figure 4a. Evaluation using 100 Monte Carlo simulations. The solid curve denotes RMSE. $u_{\max} = 2\text{m/s}^2$.

horizon generally enables foresight in the sensor maneuvers at the expense of computation. As expected we observe both better average and worst-case performance.

4.3. Six Doppler sensors tracking a single target

We now increase the complexity of the tracking problem by considering a target moving in three-dimensional space ($d = 3$) and using only Doppler frequency shift measurements. Using the states (1) in (3), we see that each Doppler sensor effectively measures the angle between the target direction vector, $(\mathbf{p}^n - \tilde{\mathbf{p}}^m) / \|\mathbf{p}^n - \tilde{\mathbf{p}}^m\|$, and the velocity difference, $(\mathbf{v}^n - \tilde{\mathbf{v}}^m)$. It is, therefore, a nontrivial task to dynamically control the sensors to maintain a good tracking performance for a moving target.

We consider $M = 6$ Doppler sensors as shown in Figure 6. The target starts moving from the top-right corner of the perimeter, following an arc-shaped trajectory along the outer boundary toward the bottom-left. Along this path, the angle between the target’s direction vector and the velocity difference changes rapidly, making the sensor responses more complex. The resulting tracking errors are shown in Figure 7.

What additional gains do we receive from dynamically moving sensors as opposed to static sensors? To study this, we repeat the experiment above but keep the sensor control disabled for $t \leq 50$. During this period, the

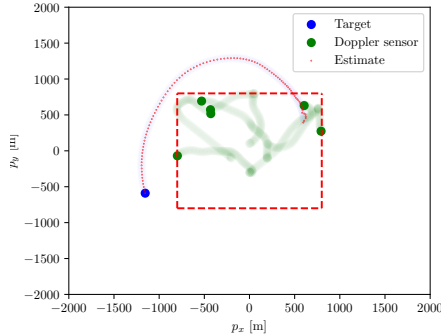


Figure 6: Tracking using $M = 6$ mobile Doppler sensors. $u_{\max} = 2 \text{ m/s}^2$ and $a_{\max} = 5 \text{ m/s}^2$. Sensor motion becomes nontrivial.

corresponding CRB and tracking error in Figure 7 stabilize at a plateau significantly higher than in the dynamically moving sensor case. However, after turning on sensor control at $t > 50$, the CRB and tracking error eventually converge to similar levels as before around $t = 100$.

4.4. Four mixed sensors tracking a single target

Additional complexity is introduced into the scenario above when we use a mix of sensor types. Figure 8a illustrates a simple case where a target follows a slow, uniform rectilinear motion. Three ranging sensors are initially positioned at different corners of the perimeter, while a fourth is placed at the center of the area. The sensor movements are straightforward to interpret—sensors will approach the target, aligning to achieve a good dilution of precision. Next, we replace one ranging sensor with a Doppler sensor, as shown in Figure 8b. As we have seen before, Doppler sensors provide ranging information through their relative motion to the target. We see that the Doppler sensor follows an intricate path, deviating from the target, taking into account both the angle and magnitude of the velocity difference to the target. As shown in Figure 9, the position errors in the two cases quickly stabilize with a slightly higher level for the mixed case as expected.

5. CONCLUSION

We have considered the problem of tracking multiple targets using mobile sensors of (possibly) different types. The proposed tracking system employs

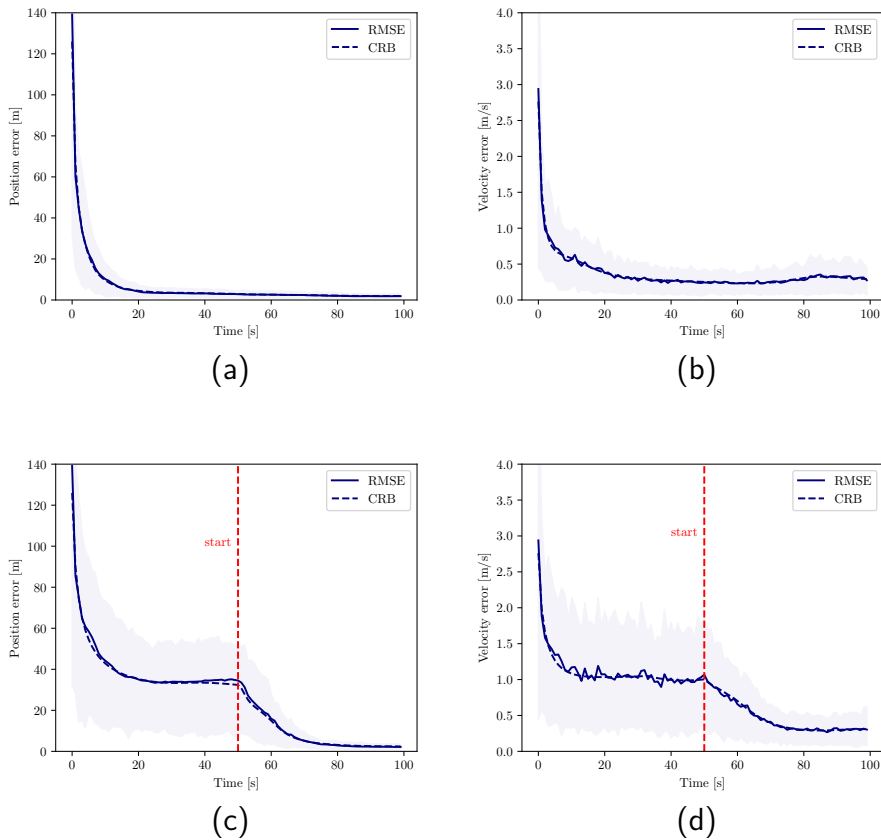


Figure 7: Tracking performance in scenario shown in Figure 6, using sensor control ((a) and (b)) versus partially static sensors ((c) and (d)). In the latter case, sensor control is turned on at $t = 50$.

minimal assumptions about the target dynamics, merely that their accelerations are bounded. The sensor control law uses a maximum likelihood estimator to determine the sensor accelerations so as to maximize target resolvability, while taking into account the uncertainty of target trajectories. The objective is posed using the expected Cramér-Rao bound. The mobile sensor control law is implemented using an efficient interior point method. The resulting method is illustrated in a series of experiments involving both round-trip time based ranging and Doppler frequency shift measurements.

The tracking system exhibits an intuitive behaviour in simple settings, such as a single target with range-only sensors. However, for mixed sensor

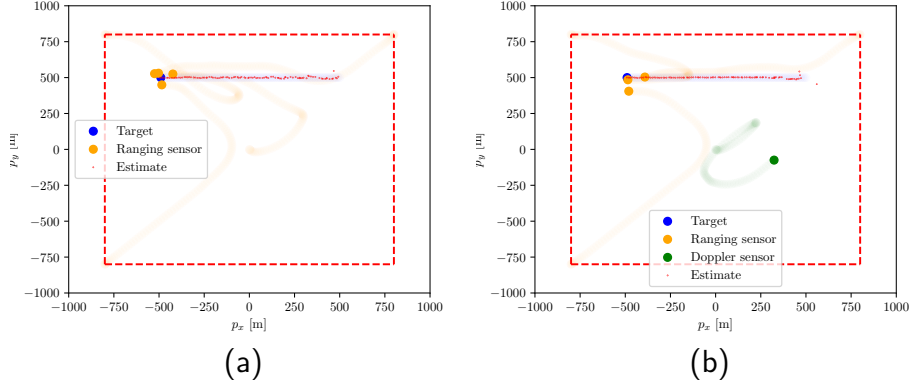


Figure 8: (a) Tracking a single target using four ranging sensors. (b) Same target but one ranging sensor is replaced by a Doppler sensor. $u_{\max} = 2 \text{ m/s}^2$ and $a_{\max} = 5 \text{ m/s}^2$.

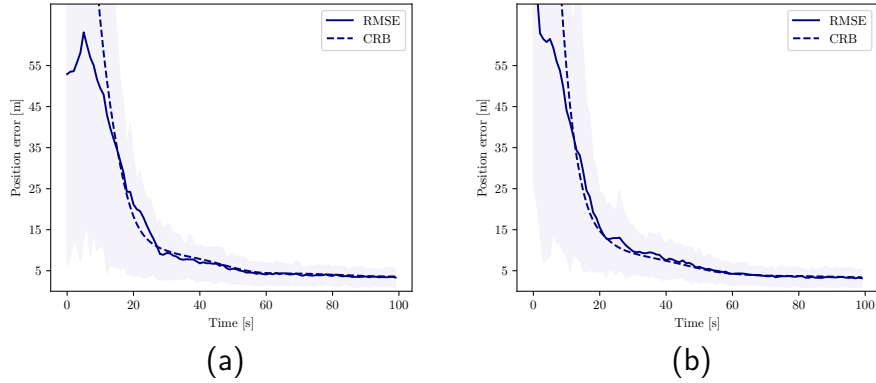


Figure 9: (a) and (b), position errors when tracking with four ranging sensors as shown in Figure 8a versus tracking with three ranging sensors and one Doppler sensor as shown in Figure 8b, using 100 Monte Carlo simulations.

types or multiple targets, the resulting sensor trajectories are nontrivial. We showed that the proposed joint estimation and control solution leads to robust tracking performance even when starting from highly challenging initial sensor configurations.

ACKNOWLEDGMENT

The authors would like to thank Dr. Torbjörn Wigren for helpful comments and advice on the simulation scenarios.

References

- [1] Yaakov Bar-Shalom, X Rong Li, and Thiagalingam Kirubarajan. *Estimation with applications to tracking and navigation: theory algorithms and software*. John Wiley & Sons, 2004.
- [2] Samuel S Blackman. Multiple hypothesis tracking for multiple target tracking. *IEEE Aerospace and Electronic Systems Magazine*, 19(1):5–18, 2004.
- [3] Guillem Brasó and Laura Leal-Taixé. Learning a neural solver for multiple object tracking. In *Proceedings of the IEEE/CVF conference on computer vision and pattern recognition*, pages 6247–6257, 2020.
- [4] James V Candy. *Bayesian signal processing: classical, modern, and particle filtering methods*, volume 54. John Wiley & Sons, 2016.
- [5] Kuo-Chu Chang and Yaakov Bar-Shalom. Joint probabilistic data association for multitarget tracking with possibly unresolved measurements and maneuvers. *IEEE Transactions on Automatic control*, 29(7):585–594, 1984.
- [6] Maria Juhlin and A Jakobsson. Optimal sensor placement for localizing structured signal sources. *Signal Processing*, page 108679, 2022.
- [7] T. Kailath, A.H. Sayed, and B. Hassibi. *Linear Estimation*. Prentice-Hall information and system sciences series. Prentice Hall, 2000. ISBN 9780130224644.
- [8] Steven M Kay. *Fundamentals of statistical signal processing: estimation theory*. Prentice-Hall, Inc., 1993.
- [9] Sonia Martínez and Francesco Bullo. Optimal sensor placement and motion coordination for target tracking. *Automatica*, 42(4):661–668, 2006.

- [10] Fabio Morbidi and Gian Luca Mariottini. Active target tracking and cooperative localization for teams of aerial vehicles. *IEEE transactions on control systems technology*, 21(5):1694–1707, 2012.
- [11] Jan Neering, Marc Bordier, and Nadia Maizi. Optimal passive source localization. In *2007 International Conference on Sensor Technologies and Applications (SENSORCOMM 2007)*, pages 295–300. IEEE, 2007.
- [12] Songhwai Oh, Stuart Russell, and Shankar Sastry. Markov chain monte carlo data association for multi-target tracking. *IEEE Transactions on Automatic Control*, 54(3):481–497, 2009.
- [13] Yaakov Oshman and Pavel Davidson. Optimization of observer trajectories for bearings-only target localization. *IEEE Transactions on Aerospace and Electronic Systems*, 35(3):892–902, 1999.
- [14] Sangwoo Park, Erchin Serpedin, and Khalid Qaraqe. Gaussian assumption: The least favorable but the most useful [lecture notes]. *IEEE Signal Processing Magazine*, 30(3):183–186, 2013.
- [15] Donald Reid. An algorithm for tracking multiple targets. *IEEE transactions on Automatic Control*, 24(6):843–854, 2003.
- [16] Petre Stoica and Prabhu Babu. The gaussian data assumption leads to the largest cramér-rao bound [lecture notes]. *IEEE Signal Processing Magazine*, 28(3):132–133, 2011.
- [17] Petre Stoica, Randolph L Moses, et al. *Spectral analysis of signals*, volume 452. Pearson Prentice Hall Upper Saddle River, NJ, 2005.
- [18] ShiJie Sun, Naveed Akhtar, HuanSheng Song, Ajmal Mian, and Mubarak Shah. Deep affinity network for multiple object tracking. *IEEE transactions on pattern analysis and machine intelligence*, 43(1):104–119, 2019.
- [19] H.L. Van Trees. *Detection, Estimation, and Modulation Theory: Detection, estimation, and linear modulation theory*. Detection, Estimation, and Modulation Theory. Wiley, 1968.
- [20] Andreas Wächter and Lorenz T Biegler. On the implementation of an interior-point filter line-search algorithm for large-scale nonlinear programming. *Mathematical programming*, 106(1):25–57, 2006.

- [21] Zongyao Wang and Dongbing Gu. Cooperative target tracking control of multiple robots. *IEEE Transactions on Industrial Electronics*, 59(8): 3232–3240, 2011.
- [22] Torbjörn Wigren and Sholeh Yasini. Passive uav tracking in wireless networks. *IEEE Transactions on Aerospace and Electronic Systems*, 58(5):4101–4118, 2022.
- [23] Jason L Williams and Roslyn A Lau. Data association by loopy belief propagation. In *2010 13th international conference on information fusion*, pages 1–8. IEEE, 2010.
- [24] Sheng Xu, Linlong Wu, Kutluyıl Doğançay, and Mohammad Alae-Kerahroodi. A hybrid approach to optimal toa-sensor placement with fixed shared sensors for simultaneous multi-target localization. *IEEE Transactions on Signal Processing*, 70:1197–1212, 2022.
- [25] Bin Yang. Different sensor placement strategies for tdoa based localization. In *2007 IEEE International Conference on Acoustics, Speech and Signal Processing-ICASSP'07*, volume 2, pages II–1093. IEEE, 2007.
- [26] Zhongshun Zhang and Pratap Tokekar. Tree search techniques for adversarial target tracking with distance-dependent measurement noise. *IEEE Transactions on Control Systems Technology*, 30(2):712–727, 2021.